Available online at www.sciencedirect.com
ScienceDirect
Trans. Nonferrous Met. Soc. China 28(2018) 783−793
Transactions of Nonferrous Metals Society of China
www.tnmsc.cn

Thermodynamics and kinetics of fluoride removal from simulated zinc sulfate solution by La(III)-modified zeolite

Yan-qing LAI, Kai YANG, Chao YANG, Zhong-liang TIAN, Wei-chang GUO, Jie LI

School of Metallurgy and Environment, Central South University, Changsha 410083, China

Received 28 February 2017; accepted 24 December 2017

Abstract: To understand the mechanism of fluoride removal from the simulated zinc sulfate solution by the La(III)-modified zeolite, the adsorbent was characterized by XRD, SEM and EDS. The effects of absorbent dose and contact time, the adsorption isotherms and the sorption kinetics were investigated. The experimental results were compatible with the Langmuir isotherm model. The theoretical maximum adsorption capacities are 20.83 and 23.04 mg/g at 303 and 313 K, respectively. And the physisorption is revealed using the Temkin isotherm model and the D−R isotherm model. The sorption process is more suitable by the pseudo-second-order kinetic models. Thermodynamic parameters such as standard free energy change ($\Delta G^{\ominus}$<0 kJ/mol), standard enthalpy change ($\Delta H^{\ominus}$=8.28 kJ/mol) and standard entropy change ($\Delta S^{\ominus}$=0.030 kJ/(mol·K)) indicate the spontaneity of adsorption and endothermic physical sorption. Furthermore, the fluoride concentration in the industrial zinc sulfate solution decreases from 98.05 to 44.09 mg/L with the adsorbent dosage of 15 g/L.

Key words: La(III)-modified zeolite; fluoride removal; zinc sulfate solution; adsorption isotherm; kinetics

1 Introduction

Zinc is an important non-ferrous metal in modern society, and over 80% of zinc is produced through the conventional hydrometallurgical method with oxidative roasting, acid leaching, purification, and electrowinning process(OLPE) [1]. With poor mineral reserves, ores, including zinc, struggle with the "lean, fine, miscellaneous" dilemma. In practice, the roasting and leaching processes are combined, resulting in high fluoride ion concentration in electrolyte. It can cause problems in the electrowinning system, such as anode corrosion, cathode corrosion, zinc sticking, and electrolytic zinc grade reduction [2,3]. In addition, high fluoride content can also worsen the working environment and damage the workers' health. So, the fluoride ion concentration in electrolyte needs to be reduced before reaching the electrowinning system (F<80 mg/L) [4]. In China, the fluoride concentration in the zinc electrowinning process is amended to be 50 mg/L [5].

Currently, pyrometallurgical roasting and caustic washing are widely applied to the removal of fluoride in industry. The former requires high-temperature equipment, such as multiple hearth furnaces and rotary kilns, and there are disadvantages of high cost, high energy consumption and low efficiency, while the latter produces large amounts of wastewater and the waste water must be treated by other methods [6]. There are also other ways for fluoride removal, such as chemical precipitation [7], ion exchange [8], coagulation precipitation [9] and adsorption [10]. Coagulation precipitation is difficult to be widely used in practice because of the high cost and a quite long time for treatment [5]. Ion exchange is inefficiency and high zinc loss for removing fluoride from the zinc sulfate solution. Meanwhile, it will produce large number of wastewater containing fluoride, which needs to be further treated [11]. Chemical precipitation is a traditional method to remove the fluoride, but the property of fluoride removal is limited due to performance of poor filtration [12]. In addition, silicone and some resins as adsorbents are capable of removing fluoride [13]. However, other ions in the electrolyte will be lost because of their poor selectivity.

Zeolite is microporous aluminosilicates with three-dimensional structure, which contains a lot of channels

Foundation item: Projects (51474238, 51674301) supported by the National Natural Science Foundation of China
Corresponding author: Zhong-liang TIAN; Tel: +86-731-88830649; E-mail: tianzhongliang@126.com
DOI: 10.1016/S1003-6326(18)64711-9

and pores. And it is lower price, abundance, diversity and molecular sieving [14]. So, it has been the focus of removing cationic and anionic ion. But its adsorption capacity is restrictive when it is used to remove anionic ion in the solution. And the positive ions within the channels and pores on the network are easily exchanged by other cations [15]. Therefore, to give place to active sites for the removal of fluoride and utilize stronger cationic-exchange properties, the polyvalent metals (e.g., La, Al, Zr, etc) were used to modify the zeolite to increase adsorption capacity [16,17]. Especially, lanthanum could form stable compounds with most non-metallic elements, so the La(III)-modified adsorbents will adsorb larger numbers of anionic ions [18]. Due to lower cost compared with other rare earth elements [19] and environmental friendly, nontoxic, the La(III)-modified zeolite was adopted to remove anionic ion in drinking water [17].

Therefore, the La(III)-modified zeolite was applied to removing the fluoride from the simulated zinc sulfate solution and exhibited good property in the previous studies. But compared with the efficiency of fluoride removal in drinking water, defluorination efficiency in zinc sulfate solution is limited. In this study, the common La(III)-modified zeolite fluoride removal adsorbent for the simulated zinc sulfate solution was prepared through the impregnating method. The thermodynamic and kinetic parameters were estimated. And the isotherm models and the kinetics models were investigated. The purpose is to understand the defluoridation behavior and the La(III)-modified zeolite mechanism and increase efficiency of fluoride removal from zinc sulfate solution with the La(III)-modified zeolite.

2 Experimental

2.1 Materials

The artificial zeolite sample in particle size of 850−425 μm was obtained from Sinopharm Chemical Reagent Co., Ltd., China. The sample was handled twice in deionized water at room temperature for 30 min while stirring, then filtered and dried to finish the sample pretreatment. The pre-process sample was also soaked in a 150 g/L $La(NO_3)_3$ solution at 40 °C for 4 h with a solid to solution ratio of 1:5 while stirring and then immersed at room temperature for 20 h. After filtering and drying, the La(III)-modified zeolite sample was obtained.

2.2 Batch adsorption studies

Preparation of the simulated solution (100 mg/L F^-, 160 g/L Zn^{2+}, 240 g/L SO_4^{2-}) was done by dissolving 0.221 g anhydrous sodium fluoride and 715 g $ZnSO_4{\cdot}7H_2O$ in 1 L of deionized water for practical application. Then, the adsorbent with different doses was added into 100 mL of the stock solution in a glass conical flasks shaked in a thermostat water bath cauldron at a invariable speed of 150 r/min at 40 °C for 30 min. The effect of contact time ranging from 0.5 to 38 h on defluoridation was executed and the adsorption kinetics was studied in the same range of contact time. The adsorption isotherm was discussed with the initial fluoride concentrations of 20, 50, 80, 100, 150, and 200 mg/L at 30 and 40 °C at 150 r/min for a desired time. The thermodynamic parameters were estimated in the stock solution at 30, 35, 40, and 50 °C. And all experiments were performed at pH 4.59±0.02. Fluoride concentration was measured in filtrates after fluoride removal and filtering. The adsorbed fluoride capacity was estimated from

$$q_e = (\frac{\rho_0 - \rho_e}{m})V \quad (1)$$

where q_e is the adsorption capacity at equilibrium, ρ_0 and ρ_e are the initial and equilibrium fluoride concentrations in the solution, respectively, V is the volume of the solution, and m is the mass of the adsorbent used.

The efficiency (η) of fluoride ion removal by the adsorbent was defined as

$$\eta = (\frac{\rho_0 - \rho_e}{\rho_0}) \times 100\% \quad (2)$$

2.3 Characterization

The phase of the adsorbent material was performed by X-ray diffraction (XRD, Rigaku3014) with Cu/K_α radiation and scans were recorded from 10° to 75° (2θ). A high qualitatively scanning electron microscope (SEM) was used to exam the surface morphology of the zeolite and La(III)-modified zeolite. The spot elemental analyses of the zeolite and La(III)-modified zeolite were carried out using the energy dispersive X-ray spectroscopy (EDS) detector (SEM-EDS, JSM−6360LV, JEOL), respectively.

2.4 Methods of analysis

Fluoride analysis was determined by the ion-selective electrode method using an ion meter (PXSJ−216, Shanghai, Leici, China) with the fluoride ion selective electrode (PF-2-01, Shanghai, Leici, China). The triammonium citrate solution buffered the pH and background ion concentrations during measurement. pH was measured using the same ion meter with a pH electrode (E-201-C, Shanghai, Leici, China). Fluoride standard solutions with fluoride concentration ranges of 10−200 mg/L were used to obtain standard curves. The solution in the glass beaker was placed on a magnetic stirrer during measurement, while the electrode was placed in the solution. The fluoride analysis ended upon stabilization of the numerical reading displayed on the ion meter screen.

2.5 Fluoride removal from zinc sulfate electrolyte

The zinc sulfate electrolyte was collected from Yunnan Chihong Zn&Ge Co., Ltd., China. The composition of the electrolyte was measured, and the analyzed parameters were pH 4.95, Zn^{2+} concentration 125.17 mg/L, Fe^{2+} concentration 1.8 mg/L and F^{-} concentration 69.48 mg/L. To increase the fluoride concentrations of this electrolyte sample, the anhydrous sodium fluoride was added to the zinc sulfate electrolyte. The fluoride concentration was also raised by approximately 100 mg/L. The new sample was re-analyzed and reached 98.05 mg/L. The spiked electrolyte sample was treated with various adsorbent doses from 0.5 g to 1.5 g at the same contact time in different conical glass flasks, where 100 mL of the new sample was taken and mixed. After the defluoridation experiment, the solution was filtered from the solid adsorbent. Finally, the remaining fluoride in the filtrate was analyzed.

3 Results and discussion

3.1 Characterization

The XRD pattern of the La(III)-modified zeolite sample is exhibited in Fig. 1. The characteristic peaks of zeolite are observed at 2θ=15.78°, 20.33°, 23.78°, 26.28°, 29.93° and 36.64°. The XRD diffraction shows the peaks of La_2O_3 at 2θ=38.07°, 46.08°. The diffraction peaks at 2θ=35.50° and 41.99° are attributed to $La_2Si_2O_7$. And other peaks are SiO_2, Al_2O_3 and $Na_2Si_3O_7$. Figures 2(a) and (c) exhibit the SEM images of the zeolite and La(III)-modified zeolite. Compared with the zeolite, many small particles appeared on the surface of the La(III)-modified zeolite. Figure 2(b) shows the presence of Na, Mg, Al, Si, O on the surface of the zeolite. At the same time, Fig. 2(d) shows lanthanum except the original elements on the surface of the zeolite, which can be attributed to the soaking process with $La(NO_3)_3$ salt solutions. Therefore, the La(III)-modified zeolite is obtained successfully.

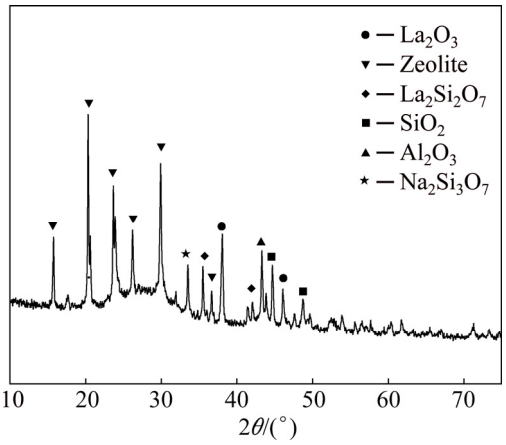

Fig. 1 XRD pattern of La(III)-modified zeolite sample

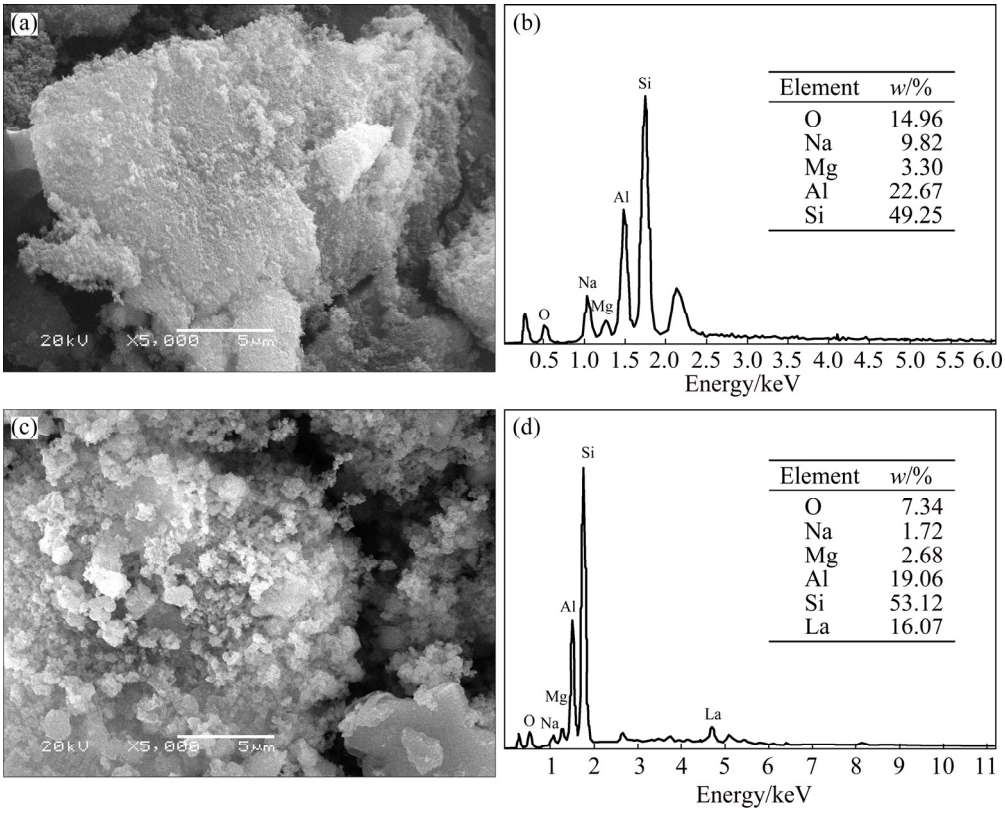

Fig. 2 SEM images (a, c) and EDS results (b, d) of zeolite (a, b) and La(III)-modified zeolite (c, d)

3.2 Effect of adsorbent dose

The effect of absorbent dose was studied at a certain initial fluoride concentration of 100 mg/L, and the result is shown in Fig. 3. It is found that the fluoride removal rate increases from 33.54% to 40.49% with an increase in adsorbent dose from 5 to 17.5 g/L after 30 min, respectively. And the fluoride removal rate increases quickly with the adsorbent dose increasing from 5 to 10 g/L. Moreover, the adsorbent dose over 10 g/L, the increase of fluoride removal is negligible and almost achieves adsorption equilibrium. Thus, 10 g/L of adsorbent (La(III)-modified zeolite) is fixed as the optimum dose which could reach reasonably good defluoridation efficiency.

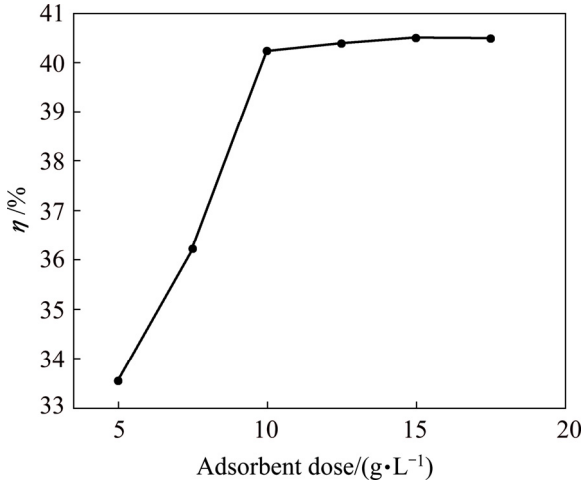

Fig. 3 Fluoride removal in simulated solution with different adsorbent (La(III)-modified zeolite) doses at (313±1) K and pH (4.59±0.02)

3.3 Adsorption capacity versus contact time

The contact time is one of the critical factors in the defluoridation process. It is researched in the range of 0.5−38 h with a dose of 10 g/L at 150 r/min and the result is presented in Fig. 4. Figure 4 indicates that the defluoridation process can be divided into two parts. From 0.5 to 3 h, the adsorption capacity of fluoride increases from 4.39 to 6.57 mg/g. After 3 h, the growth rate of the adsorption capacity of fluoride slows down and then reaches balance time at 19 h. Hence, the optimum time is fixed as 19 h.

3.4 Adsorption isotherms

Adsorption isotherms, either through theoretical or empirical equations, are essential in the basic design and operation of adsorption processes. In the present study, Langmuir, Freundlich, Temkin and Dubinin−Radushkevich (D−R) isotherm models were introduced to evaluate the mechanisms of adsorption and the maximum adsorption capacity of the adsorbent in a solid/liquid adsorption system [20]. The corresponding data are shown in Fig. 5, Tables 1 and 2.

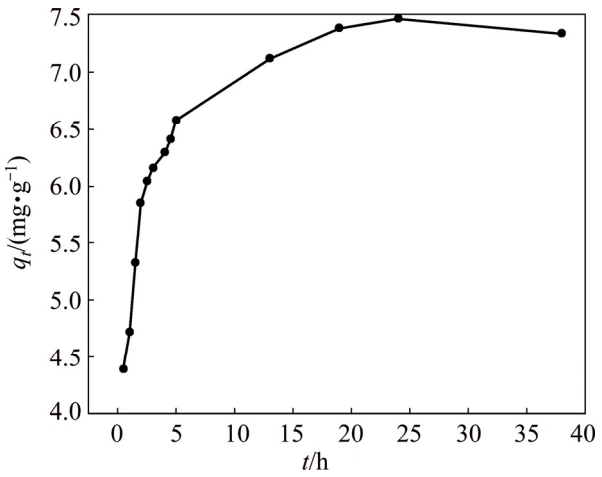

Fig. 4 Effect of contact time on fluoride removal with adsorbent (La(III)-modified zeolite) dose of 10 g/L at (313±1) K and pH (4.59±0.02) in simulated solution

The Langmuir isotherm model (Eq. (3)), which is based on monolayer adsorption on the homogeneous adsorbent surface without interaction between adsorbed molecules [21], is given as

$$\frac{1}{q_e}=\frac{1}{q_m}+\frac{1}{q_m f \rho_e} \tag{3}$$

where q_m is the maximum amount of La(III)-modified zeolite for a complete monolayer on the bound surface, and f is a constant related to the affinity of the binding sites. As shown in Table 1, the q_m and f values are calculated from the intercept and slope of the $1/\rho_e$ vs $1/q_e$ plots at 303 and 313 K (Fig. 5(a)). The separation factor (R_L) of Langmuir adsorption determines whether the adsorption is favorable. It can be obtained using (Eq. (4)) [22]:

$$R_L=\frac{1}{1+f\rho_0} \tag{4}$$

where ρ_0 is an important parameter to adsorption system prediction.

The Freundlich model (Eq. (5)) is an empirical equation based on the assumption of adsorption on the heterogeneous surface and multilayer adsorption with energetic, non-uniform distribution [23]. The model is given as

$$\ln q_e=\ln K_F+\frac{1}{n}\ln \rho_e \tag{5}$$

where K_F and n are Freundlich constants related to

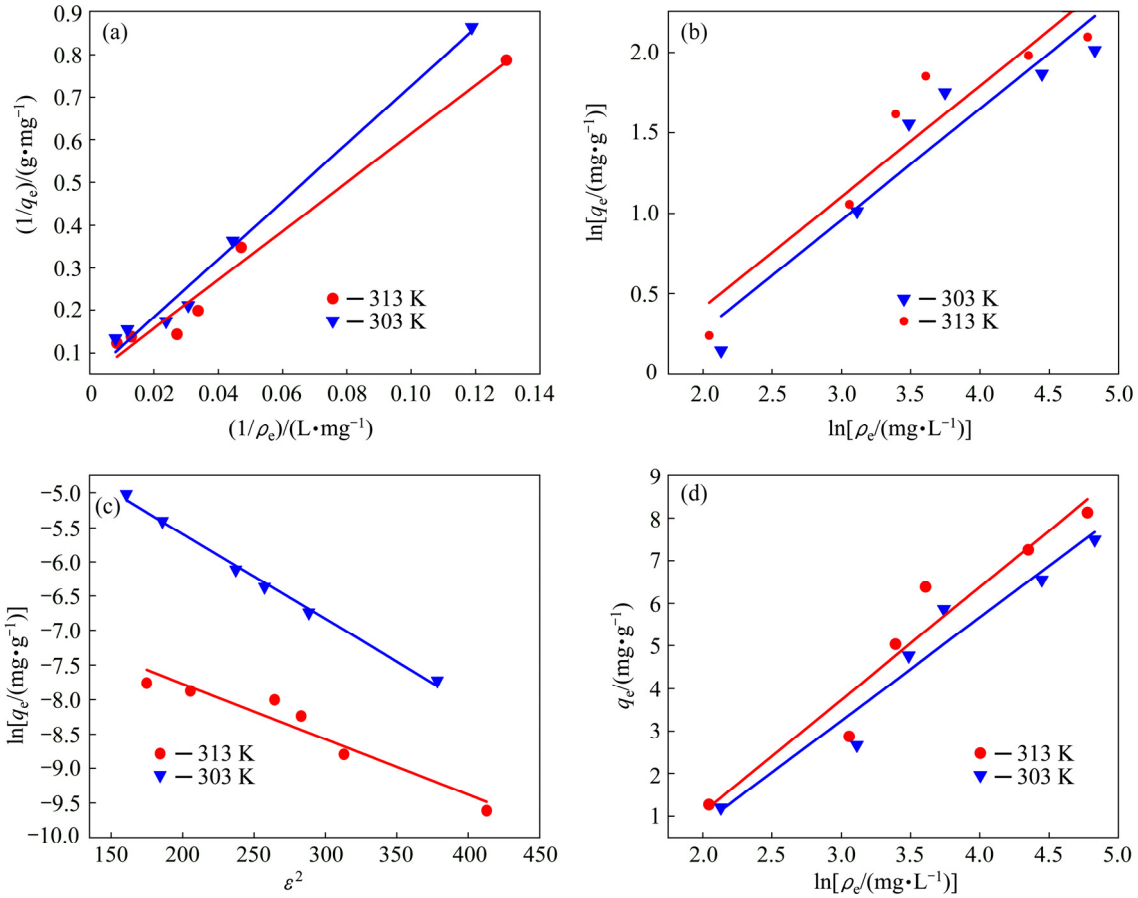

Fig. 5 Plots of Langmuir (a), Freundlich (b), Dubinin−Radushkevich (c) and Temkin (d) isotherm models for sorption of fluoride on La(III)-modified zeolite at different initial fluoride concentrations with adsorbent dose of 10 g/L at (303±1) K and (313±1) K and pH (4.59±0.02) in simulated solution

Table 1 Different isotherm parameters for adsorption of fluoride ions on La(III)-modified zeolite at (303±1) and (313±1) K

T/K	Langmuir			Freundlich		
	q_m/(mg·g^{-1})	f/(L·mg^{-1})	R^2	K_F/(mg·g^{-1})	n	R^2
303	20.83	0.0071	0.986	0.3286	1.4479	0.902
313	23.04	0.0076	0.978	0.3799	1.4491	0.890
T/K	D−R				Temkin		
	Q_D/(mol·g^{-1})	B_D/(mol·kJ^{-2})	E/(kJ·mol^{-1})	R^2	A_T/(L·g^{-1})	B_T/(kJ·mol^{-1})	R^2
303	0.0442	0.012	6.455	0.995	0.1898	2.423	0.945
313	0.00212	0.008	7.906	0.922	0.2044	2.644	0.935

Table 2 Values of R_L obtained from Langmuir constant f at different initial fluoride concentrations for La(III)-modified zeolite at (303±1) and (313±1) K

$\rho_{(F^{-1})}$/(mg·L^{-1})	R_L	
	303 K	313 K
20	0.8757	0.8681
50	0.7380	0.7246
80	0.6378	0.6219
100	0.5747	0.5681
150	0.4843	0.4673
200	0.4132	0.3968

adsorption capacity and absorption intensity, or surface heterogeneity, respectively. As shown in Table 1, the K_F and $1/n$ values are calculated from the intercept and slope of the ln ρ_e vs ln q_e plots at 303 and 313 K (Fig. 5(b)).

A comparison of the correlation coefficient (R^2) values of the Langmuir (R^2=0.978 and 0.986) and Freundlich plots (R^2=0.902 and 0.890) reveals that the former model is more suitable for the experimental data than the latter isotherm model, demonstrating favorable monolayer uniform adsorption conditions. Based on the Langmuir isotherm model, the predicted theoretical

maximum adsorption capacities of monolayer fluoride ion for La(III)-modified zeolite are 20.83 and 23.04 mg/g at 303 and 313 K, respectively. To access the fluoride removal efficiency of the La(III)-modified zeolite, a comparison of the Langmuir monolayer capacity of the present adsorbent is shown in Table 3 with some other reported materials. For $0<R_L<1$, the adsorption system will also be favorable, but it will be unfavourable when the R_L exceeds 1. Linear adsorption can be supported for $R_L=1$, and irreversible adsorption for $R_L=0$ [31]. R_L values from Table 2 increased along with the decrease of adsorbent temperature and initial fluoride concentration, suggesting an increasing affinity between fluoride and adsorbent. All R_L values ranged from 0 to 1, indicating favorable Langmuir adsorption. For the Freundlich isotherm model, the values of $1/n$ at 303 and 313 K are between 0 and 1, suggesting the favorable fluoride adsorption of the adsorbent. The values of K_F increased along with increasing temperature, showing that the fluoride adsorption capacity of the adsorbent increased along with the reaction temperature.

A comparison of the Langmuir and Freundlich isotherm models indicates that the fluoride ions were adsorbed at the monolayer region of the homogeneous adsorbent surface, thus achieving maximum adsorption capacity. However, the adsorption energy could not be calculated. The Dubinin−Radushkevich (D−R) isotherm model (Eq. (6)), which predicts whether the adsorption is physisorption or chemisorptions [32], is expressed as

$$\ln q_e = \ln Q_D + B_D\varepsilon^2 \tag{6}$$

$$\varepsilon = RT\ln(1+\frac{1}{\rho_e}) \tag{7}$$

$$E = (2B_D)^{-0.5} \tag{8}$$

where Q_D is the maximum adsorption capacity of the La(III)-modified zeolite, B_D is a coefficient related to mean sorption energy given by Eq. (6), and ε is the Polanyi potential obtained by Eq. (7). B_D can be used to estimate the free energy (E) of La(III)-modified zeolite, which is followed as Eq. (8).

The Q_D and B_D values are calculated from the intercept and slope of the $\ln q_e$ vs ε^2 plots at 303 and 313 K (Fig. 5(c)) and shown in Table 1.The high correlation coefficients (R^2=0.995 and 0.922) reflect the compatibility of the experimental data with the D–R isotherm model. Defined as the free energy change (E) when 1 mol of fluoride ion shifts to the surface of the adsorbent from the solution, the values of E are found to be 6.455 and 7.906 kJ/mol. If the E values fall below 8 kJ/mol, the adsorption process can be viewed as physical adsorption; when the E values rang from 8 to 16 kJ/mol, the adsorption process is an ion exchange [33]. In the current study, the values of E follow the former,

Table 3 Comparative assessment of Langmuir monolayer capacity (q_m) of La(III)-modified zeolite with some references available data for other adsorbents

Absorbent	q_m/ (mg·g^{-1})	Experimental condition	Ref.
Layered aluminum-based composite	5.62	pH 5.1, 323 K, industrial zinc sulfate solution, concentration:124−220 mg/L	[24]
Lanthanum hydroxide modified magnetites	1.42	pH 7.8, 303 K, aqueous solutions, concentration: 1−30 mg/L	[18]
Iron(III)–tin(IV) mixed oxide	10.47	pH (6.4±0.2), 303 K, aqueous solutions, concentration: 10−50 mg/L	[25]
$KMnO_4$-modified carbon	15.90	pH 2, 298 K, aqueous solutions, concentration: 5−20 mg/L	[26]
Montmorillonite	3.37	pH 6, 298 K, aqueous solutions, concentration: 2−120 mg/L	[27]
Laterite	0.85	pH 7.5, 303 K, aqueous solutions, concentration: 10−50 mg/L	[28]
Magnetic-chitosan	22.49	pH (7.0±0.2), 293 K, aqueous solutions, concentration: 5−40 mg/L	[29]
Fe(III) modified zeolite	2.31	pH (6.7±0.3), room temperature, aqueous solutions, concentration: 5−40 mg/L	[30]
La(III)-modified zeolite	20.83	pH (4.59±0.02), 303 K, simulated zinc sulfate solution, concentration: 20−200 mg/L	This work
La(III)-modified zeolite	23.04	pH (4.59±0.02), 313 K, simulated zinc sulfate solution, concentration: 20−200 mg/L	This work

suggesting that the fluoride adsorption of La(III)-modified zeolite is physisorption because of the weak Van der Waals force.

The Temkin isotherm model (Eq. (9)) was studied to investigate the influence of indirect adsorbent– adsorbate relationship on adsorption isotherms. It can be written as follows [34]:

$$q_e = B_T \ln A_T + B_T \ln \rho_e \quad (9)$$

where A_T is the binding constant and $B_T=RT/b$, b is the Temkin constant related to adsorption heat. As shown in Table 1, the B_T and A_T values are calculated from the intercept and slope of the $\ln \rho_e$ vs q_e plots at 303 and 313 K (Fig. 5(d)). Given that its correlation coefficients (R^2) are better than those of the Freundlich isotherm, the Temkin model is more compatible with the adsorbent. The values of B_T are 2.423 and 2.644 kJ/mol at 303 and 313 K, respectively. The relationship between fluoride and adsorbent is weak because of the values of B_T<8. It is suggested that the adsorption process of fluoride ions is expressed as physisorption [35], And the B_T values (the heat of adsorption of fluoride) increase along with increasing temperature, indicating that adsorption of fluoride is endothermic adsorption [36].

3.5 Adsorption kinetics

The fluoride adsorption kinetics was studied to evaluate the mechanisms of fluoride adsorption by the La(III)-modified zeolite, which controls the adsorption step. And the pseudo-first-order, pseudo-second-order and intra-particle diffusion models are used to examine the experiment data at the initial fluoride concentration of 100 mg/L. Relevant data are shown in Fig. 6 and Table 4.

The pseudo-first-order kinetics is described by [37]

$$\ln(q_e - q_t) = \ln q_e - k_1 t \quad (10)$$

where q_t is the fluoride adsorption capacities of the La(III)-modified zeolite at time t, and k_1 is the pseudo-first-order rate constant. As shown in Table 4, the pseudo-first-order rate constant (k_1) and q_e are found from the intercept and slope of the $\ln (q_e-q_t)$ vs t plots at 313 K (Fig. 6(a)).

The pseudo-second-order rate equation is expressed as [37]

$$\frac{t}{q_t} = \frac{1}{k_2 q_e^2} + \frac{t}{q_e} \quad (11)$$

$$h = k_2 q_e^2 \quad (12)$$

where k_2 is the pseudo-second- order rate constant, and h is the initial adsorption rate. As shown in Table 4, the pseudo-second-order rate constant (k_2) and q_e are calculated from the intercept and slope of the t/q_t vs t plots at 313 K (Fig. 6(b)). In Table 4, the correlation coefficients (R^2) of the pseudo-first-order and pseudo-second-order models are obtained as 0.960 and 0.999 respectively, exceeding 0.95. The k_1 and k_2 values are found to be 0.068 h^{-1} and 0.224 g/(mg·h), respectively, that are far lower compared with those of drinking water. These values can be influenced by other ions of the simulated solution. However, the calculated q_e from the

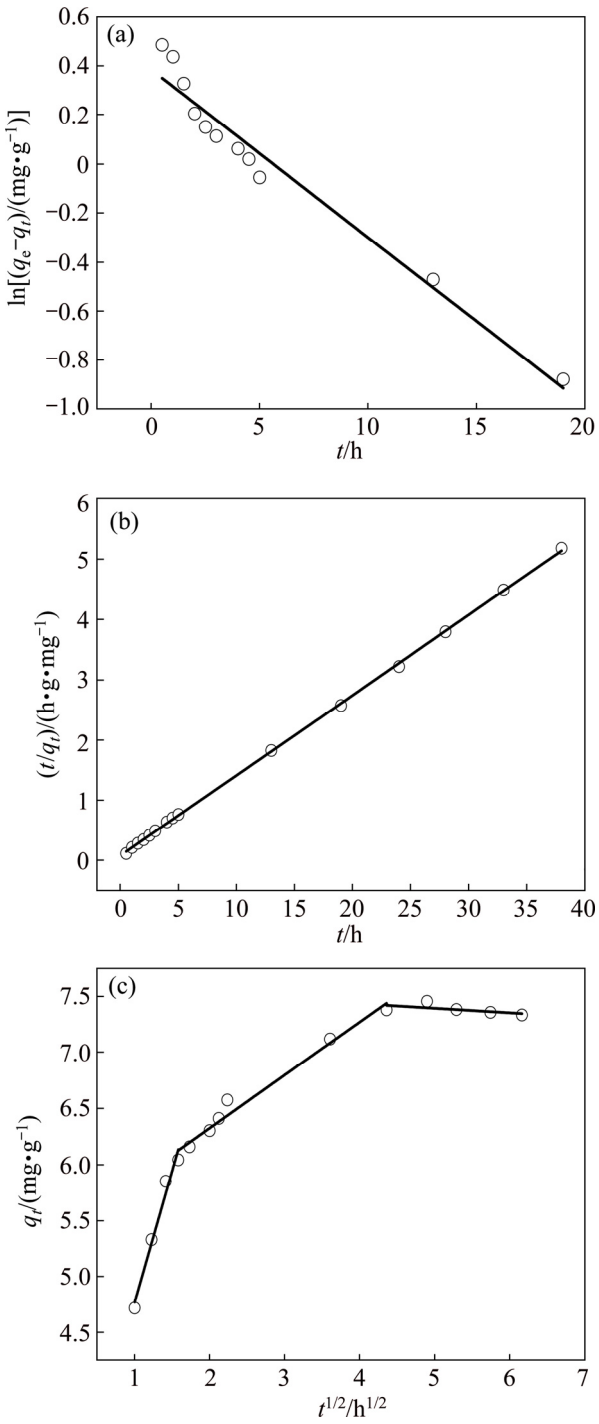

Fig. 6 Pseudo-first order (a), pseudo-second order (b) and intra-particle diffusion (c) kinetic models at initial fluoride concentration of 100 mg/L with 10 g/L La(III)-modified zeolite at (313±1) K and pH (4.59±0.02) in simulated solution

Table 4 Various kinetic parameters for fluoride adsorption on La(III)-modified zeolite at initial fluoride concentration of 100 mg/L at (313±1) K

$q_{e(exp.)}$/(mg·g^{-1})	Pseudo-first order			Pseudo-second order			
	$q_{e(cal.)}$/(mg·g^{-1})	k_1/h^{-1}	R^2	$q_{e(cal.)}$/(mg·g^{-1})	k_2/(g·mg^{-1}·h^{-1})	h/(mg·g^{-1}·h^{-1})	R^2
7.379	1.468	0.068	0.960	7.507	0.224	12.626	0.999

pseudo-first-order is lower than the experimental one, whereas that from the pseudo-second-order is closer to it. Hence, the fluoride adsorption of La(III)-modified zeolite and the experimental results are more suitable to the pseudo-second-order model. The maximum adsorption capacity from the pseudo-second-order model is less than that of the Langmuir isotherm because of the different initial fluoride concentrations. The initial adsorption rate is 12.626 mg/(g·h).

While the pseudo-first-order and pseudo-second-order models can describe the diffusion mechanism, the rate-limiting step of an adsorption process can be determined by the intra-particle diffusion model [32]. The rate constant for intra-particle diffusion can be predicted by

$$q_t = k_i t^{1/2} + C \tag{13}$$

where k_i is the intra-particle diffusion rate constant, and C provides the boundary layer thickness. Intra-particle diffusion rate constant (k_i) and C are obtained from the intercept and slope of the q_t vs $t^{1/2}$ plots at 313 K (Fig. 6(c)). If the plotted lines pass through zero, the intra-particle diffusion will define only the rate-controlling process [26]. However, the experimental data show all three lines; three steps exist in the adsorption process, including the initial curved portion, the intermediate linear portion, and a plateau. The linear fitting equations are presented as

$$q_t = 2.350t^{1/2} + 2.418 \quad (R^2=0.965,\ \text{for}\ t\leq 2) \tag{14}$$

$$q_t = 0.472t^{1/2} + 5.379 \quad (R^2=0.973,\ \text{for}\ 2<t\leq 19) \tag{15}$$

$$q_t = -0.041t^{1/2} + 7.597 \quad (R^2=0.187,\ \text{for}\ t>19) \tag{16}$$

The first linear portion indicates the existing external surface adsorption. The rate constant (k_i) and the boundary layer thickness (C) are obtained from the slope and the intercept of Eq. (14), and the values are 2.350 mg/(g·h$^{1/2}$) and C=2.418 for $t\leq 2$. The second stage implies that the micro pore diffusion obtained at $2<t\leq 19$, and the rate constant (0.472 mg/(g·h$^{1/2}$)) is calculated from the slope of Eq. (15). The rate constant is lower than the first stage. The last stage shows that equilibrium adsorption can begin after 19 h, and $C=q_e$=7.597 mg/g is closer to that of the pseudo-second order. The R^2 values of the first two stages are high, which indicates that the data are fitted with the model. The R^2 value of the last stage is low, although the data are already balanced. So, the fluoride is transported by intra-particle diffusion into the particles and is adsorbed in the pores [26]. Nevertheless, the linear portion does not pass through the origin. This indicates that the fluoride adsorption onto La(III)-modified zeolite is rather complex process and that other possible rate-controlling steps exist.

3.6 Thermodynamic analysis

To investigate the influence of temperature on the defluorination process using La(III)-modified zeolite, different thermodynamic parameters, such as standard free energy change (ΔG^Θ), standard enthalpy change (ΔH^Θ), and standard entropy change (ΔS^Θ), are estimated as

$$K_\alpha = \frac{q_e}{\rho_e} \tag{17}$$

$$\Delta G^\Theta = \Delta H^\Theta - T\Delta S^\Theta \tag{18}$$

$$\ln K_\alpha = \frac{\Delta S^\Theta}{R} - \frac{\Delta H^\Theta}{RT} \tag{19}$$

where K_α is the equilibrium constant, T is the thermodynamic temperature and R is the mole gas constant, ΔS^Θ is the standard entropy change, ΔH^Θ is the standard enthalpy change and ΔG^Θ is the standard free energy change. As shown in Fig. 7, the $\Delta S^\Theta/R$ and $\Delta H^\Theta/R$ values are calculated from the intercept and slope of the $\ln K_a$ vs $1/T$ on the Van't Hoff plot. Table 5 shows the thermodynamic parameters at various temperatures. The correlation coefficients (R^2=0.985) from Fig. 7 reflects good linearity with the plot. The positive ΔH^Θ value suggests the natural endothermic process of defluorination on La(III)-modified zeolite. For the enthalpy of adsorption, the values ranged from 8 to 25 kJ/mol, suggesting physical sorption, while the values that ranged from 83 to 830 kJ/mol indicate chemical sorption. According to the ΔH^Θ value in Table 5, the defluorination process is mainly physical sorption. The positive ΔS^Θ value also indicates increasing randomness during the defluorination step. This randomness may be explained by the increase of species at the solid–liquid interface from the release of aqua molecules and hydroxide ion when the fluoride ion is adsorbed [25,34]. The small and negative ΔG^Θ values indicate the natural adsorption spontaneity, while the increase of the ΔG^Θ with the decrease of temperature suggests that the defluorination process could be carried out difficultly at

lower temperatures [38]. So, the thermodynamic parameters indicate that the process of defluorination is spontaneous and endothermic.

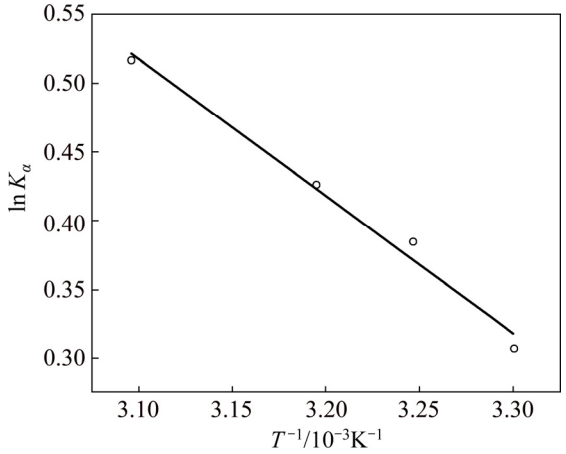

Fig. 7 Plotting of ln K_α versus $1/T$ on fluoride adsorption by La(III)-modified zeolite

Table 5 Thermodynamic parameters of sorption of fluoride on La(III)-modified zeolite

ΔS^Θ/	ΔH^Θ/	ΔG^Θ(kJ·mol^{-1})			
(kJ·mol^{-1}·K^{-1})	(kJ·mol^{-1})	303 K	308 K	313 K	323 K
0.030	8.28	−0.81	−0.96	−1.11	−1.41

4 Test with zinc sulfate electrolyte

To examine the result in zinc sulfate solution, La(III)-modified zeolite was applied to the zinc sulfate solution from the industry. Figure 8 shows the effect of fluoride ion removal from the zinc sulfate electrolyte sample (98.05 mg/L with added fluoride concentration). The defluorination efficiency clearly increases with the increase of the adsorbent dose. According to Fig. 8, with the adsorbent dose increasing from 5 to 15 g/L, the defluorination efficiency increases from 11.36% to 55.01%. With the adsorbent dose of 15 g/L, the fluoride concentration decreases to 44.09 mg/L, which is below the industrial level of fluoride concentration (50 mg/L). Compared with the rate of the fluoride ion removal from the simulated zinc sulfate solution, the speed of fluoride removal from the zinc sulfate electrolyte sample is very slow. This might be because of the competing ions present in the zinc sulfate electrolyte sample and compete with the fluoride in the zinc sulfate electrolyte sample.

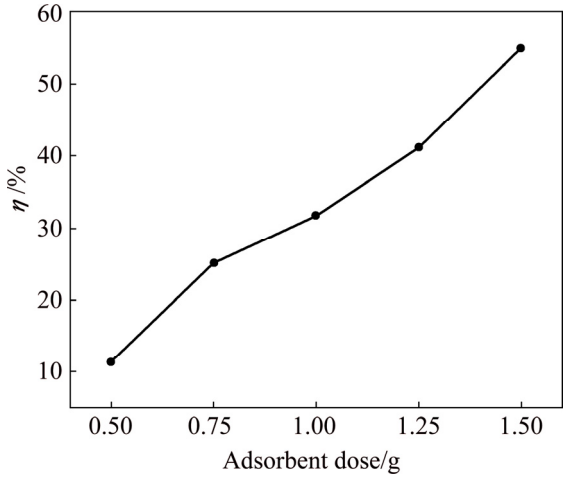

Fig. 8 Fluoride removal in zinc sulfate electrolyte with different adsorbent doses by La(III)-modified zeolite at (313±1) K

5 Conclusions

1) The La(III)-modified zeolite is performed by XRD, SEM, EDS, and the optimum adsorption conditions are determined. Under equilibrium, fluoride adsorption capacity exceeds 7 mg/g in the simulated solution (initial fluoride concentration of 100 mg/L).

2) The kinetic study suggests that the fluoride adsorption by La(III)-modified zeolite is compatible with the pseudo-second-order kinetic model, although the rate-limiting step is complex, as revealed by the intra-particle diffusion model.

3) The experimental data agree well to Langmuir isotherms model than the Freundlich, indicating monolayer uniform adsorption. And the theoretical maximum adsorption capacities were 20.83 and 23.04 mg/g at 303 and 313 K, respectively. The Dubinin−Radushkevich (D−R) and Temkin isotherm models suggest that the fluoride adsorption process is predominantly physisorption by the van der Waals force and fluoride removal is endothermic adsorption.

4) The values of ΔH^Θ, ΔS^Θ, and ΔG^Θ reveal the natural spontaneity of defluorination by La(III)-modified zeolite and its endothermic process.

5) The adsorbent also decreases the fluoride concentration of the zinc sulfate electrolyte sample (98.05 mg/L with added fluoride concentration) to 44.09 mg/L with the dosage of 15 g/L. La(III)-modified zeolite successfully adsorbs fluoride from the zinc sulfate solution before the zinc electrowinning process.

References

[1] TURAN M D, ALTUNDOĞAN H S, TÜMEN F. Recovery of zinc and lead from zinc plant residue [J]. Hydrometallurgy, 2004, 75: 169−176.

[2] LASHGARI M, HOSSEINI F. Lead-silver anode degradation during zinc electrorecovery process: chloride effect and localized damage [J]. Journal of Chemistry, 2013, 2013: 1−5.

[3] GÜRESIN N, TOPKAYA Y A. Dechlorination of a zinc dross [J]. Hydrometallurgy, 1998, 49(1−2): 179−187.

[4] LI Zhi-qiang, ZHANG Li-bo, CHEN Guo, PENG Jin-hui, ZHOU Lie-xing, YIN Shao-hua, LIU Chen-hui. Removal of fluorides and chlorides from zinc oxide fumes by microwave sulfating roasting [J]. High Temperature Materials and Processes, 2015, 34: 1−7.

[5] YU Juan, YANG Hong-ying, LI Lin-bo, CUI Ya-ru, ZHU Jun. Effect of fluoride and chioride on zinc hydrometallurgical system and their removal methods [J]. Nonferrous Metals (Extractive Metallurgy), 2014, 6: 17−21. (in Chiness)

[6] LI Zhi-qiang, LI Jing, ZHANG Li-bo, PENG Jin-hui, WANG Shi-xing, MA Ai-yuan, WANG Bao-bao. Response surface optimization of process parameters for removal of F and Cl from zinc oxide fume by microwave roasting [J]. Transactions of Nonferrous Metals Society of China, 2015, 25: 973−980.

[7] HUANG C J, LIU J C. Precipitate flotation of fluoride- containing wastewater from a semiconductor manufacturer [J]. Water Research, 1999, 33: 3403−3412.

[8] LIU Rui-xia, GUO Jin-long, TANG Hong-xiao. Adsorption of fluoride, phosphate, and arsenate ions on a new type of ion exchange fiber [J]. Journal of Colloid and Interface Science, 2002, 248: 268−274.

[9] PARTHASARATHY N, BUFFLE J, HAERDI W. Study of interaction of polymeric aluminium hydroxide with fluoride [J]. Canadian Journal of Chemistry, 1985, 64: 24−29.

[10] FANG Zhao, XUE Ning, LI Lin-bo, HONG Tao, KONG Hai-lin, WU Jiao-na. Performance and mechanism for de-fluorination by modified aluminum hydroxide in zinc sulfate solution [J]. Journal of Nanoscience and Nanotechnology, 2016, 16: 12470−12475.

[11] LIU Wei-zao, ZHANG Ren-yuan, LIU Zhong-qing, LI Chun. Removal of chloride from simulated zinc sulfate electrolyte by ozone oxidation [J]. Hydrometallurgy, 2016, 160: 147−151.

[12] SU Sha, CHEN Hai-qing. Research on removal of fluoride and chloride in zinc hydrometallurgy [J]. Hunan Nonferrous Metal, 2013, 29: 40−43. (in Chiness)

[13] XIE Wei-xin. Study on the removal of F^- from electrolytic zinc solution used for zinc-making in wet method [J]. Journal of Guang Xi University for Nationalities, 1996, 2: 26−30. (in Chiness)

[14] CAI Qian-qian, TURNER B D, SHENG Dai-chao, SLOAN S. The kinetics of fluoride sorption by zeolite: Effects of cadmium, barium and manganese [J]. Journal of Contaminant Hydrology, 2015, 177−178: 136−147.

[15] GÓMEZ-HORTIGÜELA L, PÉREZ-PARIENTE J, GARCÍA R, CHEBUDE Y, DÍAZ I. Natural zeolites from Ethiopia for elimination of fluoride from drinking water [J]. Separation and Purification Technology, 2013, 120: 224−229.

[16] ONYANGO M S, KOJIMA Y, AOYI O, BERNARDO E C, MATSUDA H. Adsorption equilibrium modeling and solution chemistry dependence of fluoride removal from water by trivalent-cation-exchanged zeolite F-9 [J]. Journal of Colloid and Interface Science, 2004, 279: 341−350.

[17] SAMATYA S, YÜKSEL Ü, YÜKSEL M, KABAY N. Removal of fluoride from water by metal ions (Al^{3+}, La^{3+} and ZrO^{2+}) loaded natural zeolite [J]. Separation Science and Technology 2007, 42: 2033−2047.

[18] GARCÍA-SÁNCHEZ J J, SOLACHE-RÍOS M, MARTÍNEZ-GUTIÉRREZ J M, ARTEAGA-LARIOS N V, OJEDA-ESCAMILLAC M C, RODRÍGUEZ-TORRESA I. Modified natural magnetite with Al and La ions for the adsorption of fluoride ions from aqueous solutions [J]. Journal of Fluorine Chemistry, 2016, 186: 115−124.

[19] SHIN E W, KARTHIKEYAN K G, TSHABALALA M A. Orthophosphate sorption onto lanthanum-treated lignocellulosic sorbents [J]. Environmental Science & Technology 2005, 39: 6273−6279.

[20] TIAN Zhong-liang, GUO Wei-chang, ZHANG Zhi-jiang, LAI Yan-qing, YE Shao-long, LI Jie. Removal of fluorine ions from industrial zinc sulfate solution by a layered aluminum-based composite [J]. Hydrometallurgy, 2017, 171: 222−227.

[21] BISWAS K, GUPTA K, GHOSH U C. Adsorption of fluoride by hydrous iron(III)–tin(IV) bimetal mixed oxide from the aqueous solutions [J]. Chemical Engineering Journal, 2009, 149: 196−206.

[22] DAIFULLAH A A, YAKOUT S M, ELREEFY S A. Adsorption of fluoride in aqueous solutions using KMnO4-modified activated carbon derived from steam pyrolysis of rice straw [J]. Journal of Hazardous Materials, 2007, 147: 633−643.

[23] TOR A. Removal of fluoride from an aqueous solution by using montmorillonite [J]. Desalination, 2006, 201: 267−276.

[24] SARKAR M, BANERJEE A, PRAMANICK P P, SARKAR A R. Use of laterite for the removal of fluoride from contaminated drinking water [J]. Journal of Colloid and Interface Science, 2006, 302: 432−441.

[25] MA Wei, YA Fei-qun, HAN Mei, WANG Ren. Characteristics of equilibrium, kinetics studies for adsorption of fluoride on magnetic-chitosan particle [J]. Journal of Hazardous Materials 2007, 143: 296−302.

[26] SUN You-bao, FANG Qing-hua, DONG Jun-ping, CHENG Xiao-wei, XU Jia-qiang. Removal of fluoride from drinking water by natural stilbite zeolite modified with Fe(III) [J]. Desalination, 2011, 277: 121−127.

[27] GOGOI S, DUTTA R K. Fluoride removal by hydrothermally modified limestone powder using phosphoric acid [J]. Journal of Environmental Chemical Engineering, 2016, 4: 1040−1049.

[28] CHEN Nan, ZHANG Zhen-ya, FENG Chuan-ping, LI Miao, CHEN Rong-zhi, SUGIURA N. Investigations on the batch and fixed-bed column performance of fluoride adsorption by Kanuma mud [J]. Desalination, 2011, 268: 76−82.

[29] WANG Yu, CHEN Ning-ping, WEI Wei, CUI Jing, WEI Zheng-gui. Enhanced adsorption of fluoride from aqueous solution onto nanosized hydroxyapatite by low-molecular-weight organic acids [J]. Desalination, 2011, 276: 161−168.

[30] BARATHI M, KUMAR A S, RAJESH N. A novel ultrasonication method in the preparation of zirconium impregnated cellulose for effective fluoride adsorption [J]. Ultrasonics Sonochemistry, 2014, 21: 1090−1099.

[31] SENTURK H B, OZDES D, GUNDOGDU A, DURAN C, SOYLAK M. Removal of phenol from aqueous solutions by adsorption onto organomodified Tirebolu bentonite: Equilibrium, kinetic and thermodynamic study [J]. Journal of Hazardous Materials, 2009, 172: 353−362.

[32] MOURABET M, BOUJAADY H E, RHILASSI A E, RAMDANE H, BENNANI-ZIATNI M, EL HAMRI R, TAITAI A. Defluoridation of water using Brushite: Equilibrium, kinetic and thermodynamic studies [J]. Desalination, 2011, 278: 1−9.

[33] NIGUSSIE W, ZEWGE F, CHANDRAVANSHI B S. Removal of excess fluoride from water using waste residue from alum manufacturing process [J]. Journal of Hazardous Materials, 2007, 147: 954−963.

[34] SEPEHR M N, SIVASANKAR V, ZARRABI M, KUMAR M S. Surface modification of pumice enhancing its fluoride adsorption capacity: An insight into kinetic and thermodynamic studies [J]. Chemical Engineering Journal, 2013, 228: 192−204.

[35] BHAUMIK R, MONDAL N K. Adsorption of fluoride from aqueous solution by a new low-cost adsorbent: Thermally and chemically activated coconut fibre dust [J]. Clean Technologies and Environmental Policy, 2015, 17: 2157−2172.

[36] BASAR C A. Applicability of the various adsorption models of three dyes adsorption onto activated carbon prepared waste apricot [J]. Journal of Hazardous Materials, 2006, 135: 232−241.

[37] POINERN G E, GHOSH M K, NG Y J, ISSA T B, ANAND S, SINGH P. Defluoridation behavior of nanostructured hydroxyapatite synthesized through an ultrasonic and microwave combined technique [J]. Journal of Hazardous Materials, 2011, 185: 29−37.

[38] OGUZ E. Equilibrium isotherms and kinetics studies for the sorption of fluoride on light weight concrete materials [J]. Colloids and Surfaces A: Physicochemical and Engineering Aspects, 2007, 295: 258−263.

La(III)改性沸石脱除模拟硫酸锌溶液中氟离子的热力学和动力学

赖延清，杨 凯，杨 超，田忠良，郭伟昌，李 劼

中南大学 冶金与环境学院，长沙 410083

摘 要：为了明确 La(III)改性沸石脱除模拟硫酸锌溶液中氟离子的机理，利用 XRD、SEM 和 EDX 对吸附剂进行表征，研究吸附剂用量和吸附时间对吸附过程的影响，采用吸附等温线与吸附动力学对吸附过程进行探究。结果表明，Langmuir 吸附等温线模型更适合吸附过程；在 303 和 313 K 条件下，吸附剂的最大理论吸附容量分别为 20.83 和 23.04 mg/g；Temkin 和 D−R 吸附等温线模型证明氟离子脱除过程为物理吸附，且吸附过程遵从准二级动力学模型；同时，热力学计算结果($\Delta G^{\ominus}$<0 kJ/mol, $\Delta H^{\ominus}$=8.28 kJ/mol, $\Delta S^{\ominus}$=0.030 kJ/(mol·K))说明 La(III)改性沸石脱除模拟硫酸锌溶液中氟离子是自发、吸热的物理过程；将 La(III)改性沸石应用在工业硫酸锌溶液中，用量为 15 g/L 时，氟离子浓度从 98.05 mg/L 降低至 44.09 mg/L。

关键词：La(III)改性沸石；脱氟；硫酸锌溶液；吸附等温线；动力学

(Edited by Xiang-qun LI)